CERN-INTC-2015-046 / INTC-P-447
14/10/2015

EUROPEAN ORGANIZATION FOR NUCLEAR RESEARCH

Proposal to the ISOLDE and Neutron Time-of-Flight Committee

Gamow-Teller decays of beta delayed neutron emitters $^{82-86}$Ga and shell effects

October 14, 2015

R. Grzywacz[1,2], M. Madurga[3], G. Benzoni [4] M.J.G. Borge[3], N.T. Brewer[2], J.A. Cizewski[5], L.M. Fraile[6], A. Gottardo[7], C.J. Gross[2], S. Go[1], S.V. Ilyushkin[8],Z. Janas[9], K. Kolos [10], M. Karny[9], A. Keeler[1], A. Korgul[9], R. Lica[3], C. Mazzocchi[9], K. Miernik[9], S.V. Paulauskas[1], W.A. Peters[1,2,10], M. Pfützner[9], K.P. Rykaczewski[2], S. Taylor[1], O. Tengblad[11], N Warr[12], H.De Witte[13],

[1] *Dept. of Physics and Astronomy, University of Tennessee, Knoxville, Tennessee 37996, USA.*
[2] *Physics Division, Oak Ridge National Laboratory, Oak Ridge, Tennessee 37830, USA.*
[3] *CERN, CH-1211 Geneva 23, Switzerland.*
[4] *INFN sezione di Milano, Dipartimento di Fisica, 20133 Milano, Italy*
[5] *Dept. of Physics and Astronomy, Rutgers University, New Brunswick, NJ 08903 USA.*
[6] *Departamento de Fisica, Universidad Complutense de Madrid, Spain*
[7] *Institut de Physique Nucléaire,CNRS/IN2P3, F91406 Orsay Cedex, France*
[8] *Department of Physics, Colorado School of Mines, Golden CO 80401.*
[9] *Faculty of Physics, University of Warsaw, PL 00-681 Warsaw, Poland*
[10] *Joint Institute for Heavy-Ion Research, Oak Ridge, Tennessee 37831, USA.*
[11] *Instituto de Estructura de la Materia, CSIC, E-28006 Madrid, Spain.*
[12] *Institut fuer Kernphysik, Universitaet zu Koeln, Germany*
[13] *Instituut voor Kern-en Stralingsfysica, KU Leuven, B-3001 Leuven, Belgium.*

Spokesperson: [Robert Grzywacz,Miguel Madurga]
[rgrzywac@utk.edu,miguel.madurga.flores@cern.ch]
Contact person: [Miguel Madurga] [mmadurga]

Abstract: We propose to study β decays of neutron rich $^{82-86}$Ga to probe the effect of shell structure on the β-decay half-lives. The Versatile Array of Netron Detectors at Low-Energies (VANDLE) will be used to measure their β-delayed neutron emission in combination with the four clover array at the ISOLDE Decay Station. This will be able to reconstruct the Gamow-Teller strength distribution to states located above the neutron separation energy. The main purpose of the experiment is to measure the persistence of the N=50 shell closure in very neutron rich nuclei. The experiment will attempt, for the first time, to measure the energy distribution in the beta-delayed two-neutron emission from the ^{86}Ga precursor.

Requested shifts: [21] shifts,

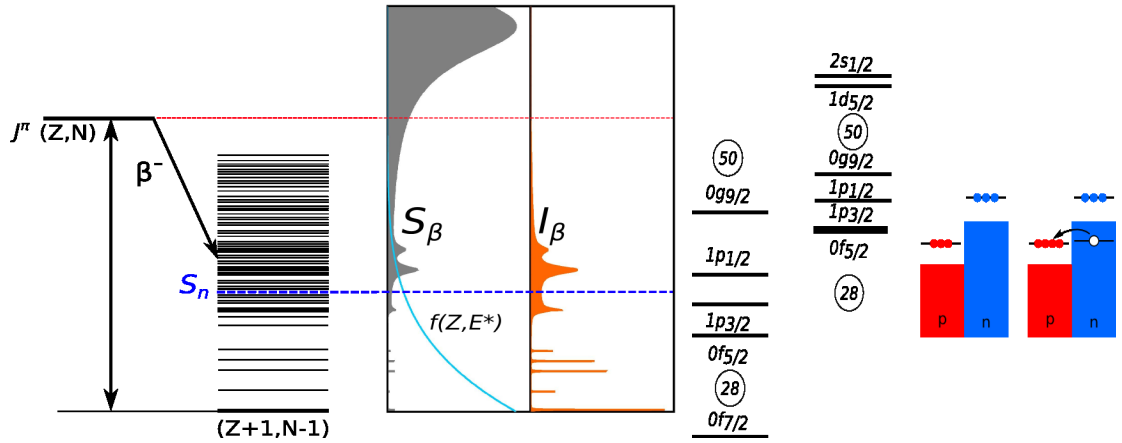

Figure 1: (Left)Diagram illustrating the connection between the measured decay branching ratios and nuclear structure. (Right)Shell model scheme near ^{78}Ni and schematic diagram, which explains the mechanism of creating highly excited states beta decay of ^{84}Ga.

1 Introduction

For the past few decades the field of nuclear physics was invigorated by the exploration into the far reaches of stability. The observation of unexpected phenomena like nuclear halos, intruder states and shape coexistence extended and refined our understanding of the nuclear force and its role organizing nuclear matter. Beta-decay properties such as the half-lives, and branching ratios were used as benchmarks for nuclear models of nuclei far from stabilty [1, 2, 3, 4]. In particular, there is a long-standing problem to realistically calculate beta-decay properties of the most neutron rich nuclei available to experimentalists. For nuclei where neutrons occupy a major harmonic shell different than the orbitals filled by protons, such as neutron rich nuclei with N>(50,82) at Z>(28,50), the decay of the valence neutrons occurs mainly through forbidden transitions. Intense Gamow-Teller decay of the "core" neutrons can be observed in such cases [5] even though they are inhibited by the large energy gap required to break the core. Moreover, neutron-rich nuclei around the major shell closures play a fundamental role in the r-process nucleosynthesis [6, 7]. Such nuclei are often difficult or impossible to access experimentally, hence the reliance of the r-process network simulations [8, 9, 10] on the global nuclear models [11, 12, 13, 14], which predict the most relevant nuclear properties: masses, lifetimes, and decay branching ratios. These observables are directly determined by various effects arising from nuclear structure. Models which aim to make credible predictions must include the relevant microscopic physics.

The connection between nuclear lifetimes and nuclear structure is made through the decay strength function S_β, see Fig. 1. The decay lifetime is, an integral of the strength functions folded with the statistical factor f over the available Q_β. This results in the obvious ambiguity inherent for nuclear models: different strength functions may produce identical lifetimes. Thus, a much better test for nuclear models is a direct comparison of the theoretical strength function with the experimental, which can be obtained from

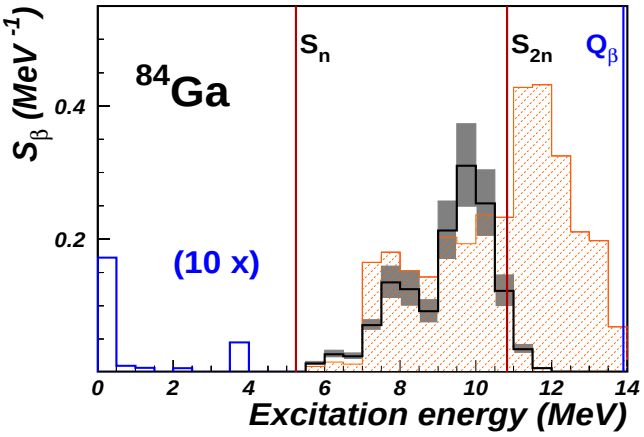

Figure 2: (Top)Gamow-Teller strength distribution above the neutron separation energy in the decay of ^{84}Ga (black solid line). The grey shaded parts of the histogram indicates the uncertainties of the measuered strength distribution. The blue part of the histogram shows the strength distribution extracted from beta delayed gamma-ray spectroscopy [22]. This histogram is multiplied by 10 in order to be visible. The dashed histogram represents shell model predictions of the Gamow-Teller strength.

experimental measurement of decay branching ratios. This topic is a subject of many past and present measurements using total absorption gamma spectroscopy studies [15]. For sufficiently neutron rich nuclei, beta decay populates neutron unbound states in the decay daughter, and neutron emission may become a dominant decay channel. This makes the neutron detection neutrons and direct measeurement of their energies critical.

The focus of this proposal is to investigate beta delayed neutron emission of the most exotic gallium isotopes: $^{82-86}$Ga. These $N > 50$ isotopes are close to the doubly magic ^{78}Ni and have large decay energy window for emission of neutrons Q_β-S_n. This enables the study of a significant portion of the Gamow-Teller strength distribution. On the practical side, gallium isotopes are the most neutron rich $N > 50$ isotopes, close to ^{78}Ni, that be easily produced at ISOL facilities [16, 17, 18, 19, 20, 21, 22] with high rates and with high purity. Associated with the large Q_β-S_n large beta-delayed neutron emission branching ratios makes them therefore the best candidates for experimental studies of beta delayed neutron emission in regions relevant for the r-process physics. The discovery of a large two-neutron emission branching ratio from ^{86}Ga [19], makes this nucleus a perfect candidate to investigate β2n emission in medium mass region of chart nuclei.

2 Gamow-Teller decays for $N > 50$ nuclei

Previous βn spectroscopy of ^{83,84}Ga revealed that neutrons are emitted at high energies and with large intensities [5]. This enabled us to conclude, that neutron unbound states are strongly populated in the Gamow-Teller decay of pf-shell neutrons. The strength distribution calculated from the data revealed a "threshold" type behavior at energies of

about 6 MeV above the ground state of the daughter nucleus. In order to explore the connection between the observed data and the underlying nuclear structure, we used shell model calculations, see Fig. 1. For these calculations we used the NushellX code [23, 24] with its built in GT transition operator. The calculations were performed within configuration space which includes proton orbital $f_{5/2}$, $p_{1/2}$ $p_{3/2}$ and $g_{9/2}$ and neutron orbitals $s_{1/2}$, $d_{5/2}$, $g_{7/2}$ and $h_{11/2}$ outside inert ^{78}Ni core. These calculations cannot reproduce the observed large beta strength disribution within the Q_β window. Within the chosen configuration space only the $\pi g_{9/2}$ and $\nu g_{7/2}$ orbitals could contribute. For N=53,54 gallium isotopes, the $\nu g_{7/2}$ contribute little to the ground state wave functions. New calculations with the larger configuration space, including additional spin-orbit partner orbitals, were performed. Here $f_{5/2}$, $p_{1/2}$ $p_{3/2}$ and $g_{9/2}$ configuration spaces for protons and neutrons were chosen with ^{56}Ni as the inert core. However, to be able to describe $N > 50$ nuclei, the orbitals from outside ^{78}Ni core have to be added. Only the $d_{5/2}$ orbital was included in order to keep numerical tractability. Most experimental and theoretical evidence points to $J^\pi = 5/2+$ ground states for even-Z and odd-N for $N > 50$ nuclei near ^{78}Ni [16]. Using a ^{56}Ni core the $d_{5/2}$ orbital has no spin orbit partners which could be populated in allowed beta decay, because the $1d_{3/2}$ single particle state is well below the Z=28 core and the $2d_{3/2}$ orbital is placed beyond Z=50 shell gap. This observation enables truncated calculations where the $d_{5/2}$ neutrons are "spectators" for the B(GT) calculations and do not directly contribute to the strength distribution. They have to be included to acccount for spin and parities of the states in the decay parent and daughter and are needed to account for the $N = 50$ shell gap effects in the beta decay of nuclei with $N > 50$. This approach was used previously to interprete the gamma-ray spectroscopy data from decays of other $N > 50$ nuclei [22, 25]. The single particle energies were taken from Grawe [26]. The size of the $N = 50$ shell-gap between $\nu d_{5/2}$ and $g_{9/2}$ is 3.9 MeV. This value is smaller by about 1 MeV than considered by other authors, see e.g. [27]. The comparison between experimental data and predictions of our model for the Gamow-Teller strength are shown in Fig. 2. In order to account for the effects of missing configuration space, the calculated B(GT) is shown using the quenching factor of 0.5 for ^{84}Ga, and compared with the experimental data [5]. The calculations reveal threshold type behavior similar to the data. The chosen 0.5 reduction of the B(GT) (quenching factor) provide a good consistency between experiment and the observation. For comparison, the strength distribution of neutron bound states is shown, which is extracted from previously published data [20]. These matrix elements are attributed to the forbidden transitions, and are so small, that they have to be multiplied by factor 10 to be visible, see Fig. 2.

Due to strong amplification by the Fermi phase space integral f, which is proportional to the fifth power of the decay energy, these transitions dominate the spectroscopy of the low energy states. However, they play a diminishing role when moving away from stability compared to the high energy Gamow-Teller transitions.

The good agreement between data and model indicates that our calculations include the most relevant physics of decay mechanisms of $N > 50$ nuclei. Valence neutrons occupying orbitals outside ^{78}Ni core contribute little to the observed Gamow-Teller strength and the high energy transformations to neutron bound states occur via weak forbidden transitions. Gamow-Teller transitions inside the Q_β window are only possible for deeply bound neutrons filling the fp orbitals. Therefore, the experimental strength distribution

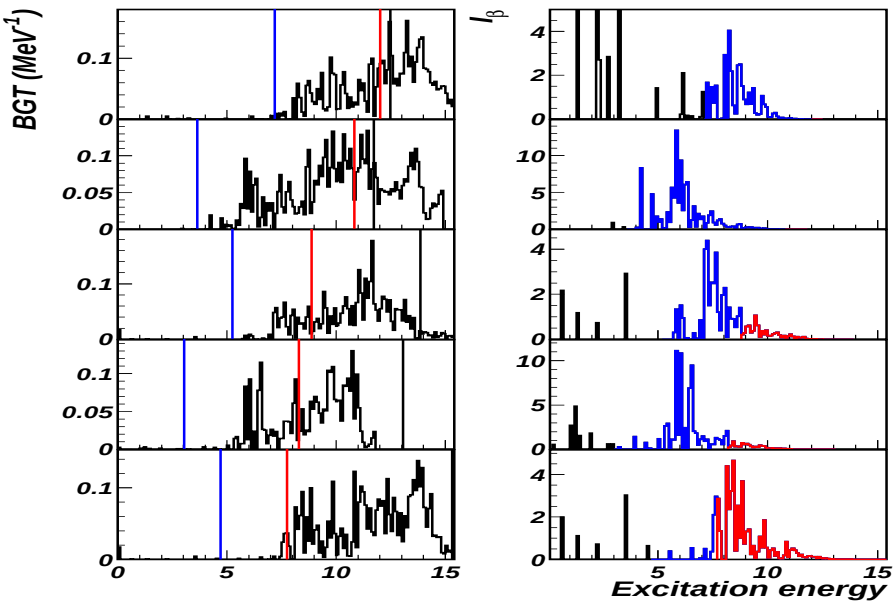

Figure 3: Shell-model calculations for $^{82-86}$Ga (left, top to bottom) and resulting beta decay feeding to the excited states (right). The vertical lines represent one-neutron (S_n)(blue) and two-neutron (S_{2n}) (red) separation energies in the decay daughter nuclei. In blue, the part of the feeding intensity to states between S_n and S_{2n} is drawn; in red, the feeding intensity to two-neutron unbound states. For comparison the expected feeding intensity to the bound states, likely due to the forbidden transitions, is shown in black.

cannot be explained by calculations using an inert ^{78}Ni core.

The agreement between the ^{83,84}Ga spectroscopic data and our large-scale shell model calculations demonstrates the unequivocal fingerprint of its underlying nuclear structure. This is in contrast with the previously held view that the neutron energy distribution followed a purely statistical behavior [28]. The lowest energy part of the B(GT), has sparse enough distribution of levels so that levels with strong B(GT) are separated and form distinct structures. These structures can be atributed to the wave-function components with particle-hole configurations, see Fig. 2. Careful inspection of the wave functions indicates that the groups of strong B(GT) are arranged around dominating transitions between spin-orbit partner orbitals. These levels are immersed in higher density of levels with drastically different structure, that do not contribute to the Gamow-Teller transformations. The density of Gamow-Teller states increases rapidly with excitation energy and at 10 MeV becomes nearly continous reaching the "pandemonium" region where the statistical description could be applied. The mixing and spreading of these states is due to the large amount of nearly degenerate configurations of states with similar spins. It is important to note that the distribution of states for any possible spin-parity do not show fluctuations as ones observed for the Gamow-Teller distribution. This distinction suggests

that the same the lowest energy B(GT) "peaks" are of great importance for the nuclear structure, because it points to the GT operator selecting only the states with paricular structure in a decay daughter.

3 Beta-delayed neutron emission from $^{82-86}$Ga

Beta delayed neutron spectroscopy of $^{83-84}$Ga was investigated at ORNL by Madurga and collaborators [5] with VANDLE array [29, 30]. The delayed neutron emission of ^{85}Ga was inferred from gamma-ray spectroscopy [21]. Finally, the beta delayed one and two neutron channels of ^{86}Ga were observed using the hybrid-3Hen detection system [19, 31]. The first implementation of VANDLE at ORNL was limited due to several factors. First ORNL VANDLE had a short time of flight distance (50 cm) in order to increase the detector efficiency to compensate for low yields. Second, the beta detector trigger was placed outside the implantation beamline, reducing the efficiency for low energy electrons due to interactions with the chamber's aluminum. Moreover, the beta "start" detectors were not optimized for timing measurements (FWHM $\sim$3.5 ns), significantly degrading overall experimental resolution. The resulting data were of sufficient quality to reconstruct the beta strength distribution highlighting the characteristic "peaks" resulting from $N = 50$ cross-shell excitations. However, the rather low time-of-flight resolution corresponded to a 0.5 MeV energy resolution. This made it impossible for the identification of single particle state feeding predicted by our calculations at energies closer to the neutrons separation energies.

VANDLE was installed at IDS in 2015, see Fig. 4 and benefitted from a series of improvements. The array is now designed for a flight path of 100 cm, improviong the energy resolution from 12% to 6%. The IDS provides a new high-efficiency (90%) in-vacuum plastic array for beta-particle detection. This array has dual PMT readout, for reduced noise and a timing resolution of $\sim$700 ps. Combining these factors we should be able to perform a much improved study of the gallium decays. The increased energy resolution will allow us to have a much better definition of the GT strength for the most neutron rich Ga isotopes, especially at low neutron energies. This provides a much more stringent test for the theoretical calculations. Here we may discuss a simple effect of the N=50 shell gap on the GT distribution. The B(GT) calculations presented here, see Fig. 3, use a constant N=50 shell gap. This results in an overall similar B(GT) distribution for decays of odd-odd and odd-even nuclei. However an evolution of the shell stucture may strongly affect the B(GT) distribution. For example, a decrease of the shell gap will lower the energy distribution B(GT) and will be reflected in an entirely different neutron spectrum. The single particle energy changes may alter the B(GT) distribution. This makes it important to have a comparative meausurements for series of odd-odd and odd-even isotopes. Strong deviations from the predicted strength distribution would indicate that shell effects play a role. In this case the measurement of decay properties of ^{86}Ga is of particular importance. This nucleus was identified to be a beta delayed two-neutron precursor with a relatively large 2n emission branching ratio of 20(10)% [19]. This branching ratio is much smaller than that predicted by our model P_n=85% (when GT only is considered). However, our calculation does not currently include a

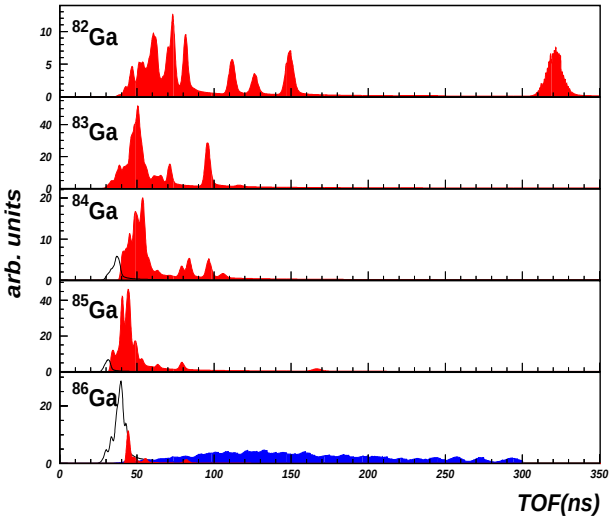

Figure 4: Simulated time of flight (TOF) spectra for one neutron emission (red) for $^{82-86}$Ga corresponding to calculated Gamow-Teller strength distributions under the assumption that the emitter decays to the ground state. The blue color shows a hypothetical distribution for two-neutron emission from two neutron unbound states in ^{86}Ge. Black color indicates the possible TOF distribution for one neutron emission from two-neutron unbound states.

microscopic particle emission model. It is expected that, for states close to the two neutron separation energy, one-neutron emission is favored due to the larger energy phase space. A recent prediction by Miernik uses schematic model of B(GT) and level densities and a statistical model to predict the competition between 1n and 2n and obtains the values of ∼50% and ∼20% for P_n and P_{2n} respectively. The shell model predictions presented here, idicate a large proportion of the B(GT) is above 2n emission threshold. Interpreted naively this would indicate a dominance of the 2 neutron emission channel. This discrepancy could be explained by a B(GT) distribution shifted to low energies, or the one-neutron emission channel might dominate for two-neutron unbound states. This has been previously observed, in the decay of ^{52}K [32]. We will address this problem by directly measuring the energy of the emitted neutron(s). The tell-tale fingerprint of one-neutron emission occurring from two neutron unbound states would be the observation of high energy neutrons. Their energies must be above at least $S_{2n}(^{86}Ge) - S_n(^{86}Ge)$=3.1 MeV, shown as a black outline in Fig. 4. If the strength is shifted down in energy, neutrons at much lower energies will be observed. For a sufficiently long experiment, VANDLE will be able to detect two neutrons in coincidence. The last panel of Fig. 4 shows their time of flight spectrum in blue. They show as an extended tail into long times of flight due to phase space energy sharing of states close to the 2-neutron separation energy. The two neutron counts may be combined into a total energy spectrum if there is enough statistics to observe both neutrons in coincidence. The observation of both neutrons in coincidence provides a first insight into the kinematics and correlations of two neutron emission for

mid-mass nuclei.

4 Beam Time request

Production of Ga isotopes is greatly enhanced at ISOLDE owing to the RILIS ion source. Expected yields [34] are presented in the table below, where the neutron shifts were calculated to measure at least 10 000 neutrons for all species. Thanks to the combination of the surface ionization source with RILIS, no contamination of neutron emitting Ge isotopes is expected. In order to avoid large intensity of gamma emitting Sr and Rb isobars produced in spallation the neutron converter source will be used. One shift of ^{49}K is requested for detector calibration.

Summary of requested shifts:

Table 1: Shift summary for the experiment. The detected neutron rates assume 90% beta detection efficiency, and VANDLE average efficiency of 6%.

Mass Number	P_n %	Rate perμC	shifts	neutrons per shift	neutrons total
82	20	5k	0.5	1.6M	0.8M
83	63	400	0.5	0.4M	0.2M
84	40	80	1	66k	66k
85	60	12	5	12k	60k
86	60	1000	13	1.5k	19.5k
49K	86	5k	1	7M	7M
Tot.			21		

References

[1] M. Pftzner *et al.*, Rev. Mod. Phys. **84**, 567 (2012).

[2] Z.Y. Xu *et al.* Phys. Rev. Lett. **113**, 032505 (2014).

[3] C.B. Hinke *et al.* Nature **486**, 341345 (2012).

[4] J.A. Winger *et al.* Phys. Rev. Lett. **102**, 142502 (2009).

[5] M. Madurga *et al.*, submitted to Phys. Rev. Lett.

[6] E. M. Burbidge, G. R. Burbidge, W. A. Fowler, and F. Hoyle. Rev. Mod. Phys. 29, 547 (1957).

[7] P.A. Seeger,W.A. Fowler, D.D. Clayton, Astrophys. J. Suppl. **11**, 12166 (1965).

[8] T. Rauscher *et al.*, Phys. Rev. C **57**, 2031(1998).

[9] R. Surman *et al.*, Astrophys. J. Lett. **77**, 035804 (2008).

[10] R. Surman *et al.*, in preparation.

[11] Möller P., Nix J.R., Kratz K.-L. Atom .Data Nucl. Data **66**, 131 (1997).

[12] P. Möller, B. Pfeiffer and K.-L. Kratz, Phys. Rev. C **67**, 055802 (2003).

[13] K. Takahashi, Prog. Theor. Phys. **45**, 1466 (1971).

[14] H. Nakata, T.Tachibana, M.Yamada, Nucl. Phys. A **625**, 521 (1997.)

[15] A.Algora *et al.*, Phys. Rev. Lett. **105**, 202501 (2010).

[16] B. Cheal *et al.*, Phys. Rev. Lett., **104**, 252502,(2010).

[17] J.A. Winger *et al.*, Phys. Rev. C **81**, 044303 (2010).

[18] M. Madurga *et al.*, Phys. Rev. Lett. **109**, 112501 (2012).

[19] K. Miernik *et al.*, Phys. Rev. Lett. **111**, 132502 (2013).

[20] K. Kolos *et al.*, Phys. Rev. C **88**, 047301 (2013).

[21] Phys. Rev. C *et al.*, **88**, 044330 (2013).

[22] M. Alshudifat *et al.*, Phys. Rev. C in press.

[23] W. Rae, NUSHELLX shell-model code, http://www.garsington.eclipse.co.uk/.

[24] B.A. Brown and W. Rae. Nuclear Data Sheets, 120, (2014).

[25] C. Mazzocchi *et al.*, Phys. Rev. C in press

[26] H. Grawe, Shell Model from a Practitioners Point of View, Lecture Notes I-II.

[27] J. Hakala *et al.*, Hakala et al. Phys. Rev. Lett. **101**, (2011).

[28] J. Hardy *et al.*, Nucl. Phys. A **305**, 15 (1978).

[29] W.A. Peters *et al.*, submitted to Nucl. Instrum Meth.

[30] S.V . Paulauskas *et al.*, Nucl. Instrum Meth. **A737**, 22 (2014).

[31] R. Grzywacz *et al.*, Act. Phys. Pol. B Vol. **45**, (2014).

[32] F. Perrot *et al.*, Phys. Rev. C 74, **014313** (2006).

[33] E. Rapisarda. Private Communication.

[34] https:oraweb.cern.chplsisoldeyield?v_url=query_tgt&v_z=31 .

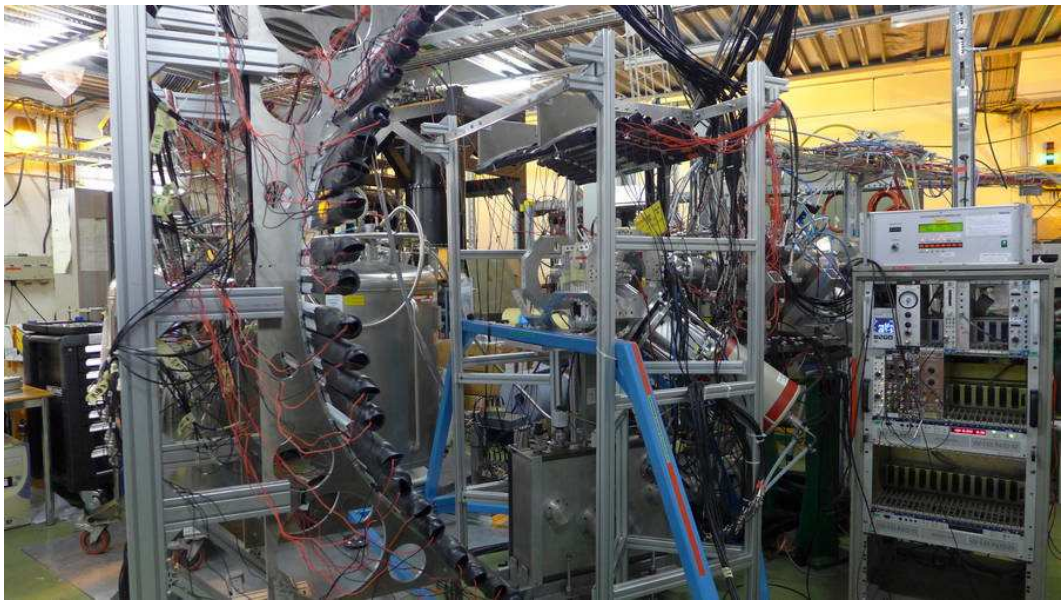

Figure 5: VANDLE at ISOLDE Decay Station during experimental campaign in 2015.

Appendix

DESCRIPTION OF THE PROPOSED EXPERIMENT The proposed experiment will utilize VANDLE at the Isolde Decay Station. A similar system was used successfully in 2015 in an experimental campaign, which measured decays of $^{51-54}$K(IS599) and ^{132}Cd(IS600). The gallium isotopes will be produced using the laser ionization technique required for beam purification. They will be implanted onto a tape, which is placed inside a beta detector, and four clover detectors will be used for detection of gamma rays. These detectors are needed for reconstruction decay energy released after beta decay. The 32 detectors of the VANDLE array will placed in 100 cm radius arc with the center at the implantation point. Neutron energies will be measured using the time-of-flight technique. The detector system will be placed using a custom-built frame surrounding a partial implementation of the ISOLDE Decay Station [33]. The VANDLE frame will be housing 32 "medium" 3x6x120 cm^3 bars. The back HPGe detectors will be removed from IDS frame for a clear view line for the VANDLE detectors. This geometry leaves a total 4% gamma efficiency at 1.3 MeV [33]. This allows us to measure the gamma transitions in the daughter nucleus and reconstruct the complete decay scheme. The modularity of VANDLE and the use of inexpensive extruded aluminium beams to build the support frame allow for to quick reconfigurations it to adapt to possible ISOLDE decay station configurations. For the typical energies in beta-delayed neutron emissions (100-4000 keV), the efficiency range is in between 20% to 50%. The angular acceptance of the full array is 18% of 4π giving a total array efficiency of 4-9% in the energy range of interest. For the neutron detection rate estimates we use a measured 90% beta detection efficiency [33]. The entire system is instrumented with Pixie-16 digital electronics due to its low energy threshold, simplicity, and stability [30].

Part of the	Availability	Design and manufacturing
(if relevant, name fixed ISOLDE installation: COLLAPS, CRIS, ISOLTRAP, MINIBALL + only CD, MINIBALL + T-REX, NICOLE, SSP-GLM chamber, SSP-GHM chamber, or WITCH)	☒ Existing	☒ To be used without any modification
[Part 1 of experiment/ equipment]	☐ Existing	☐ To be used without any modification ☐ To be modified
	☐ New	☐ Standard equipment supplied by a manufacturer ☐ CERN/collaboration responsible for the design and/or manufacturing
[Part 2 of experiment/ equipment]	☐ Existing	☐ To be used without any modification ☐ To be modified
	☐ New	☐ Standard equipment supplied by a manufacturer ☐ CERN/collaboration responsible for the design and/or manufacturing
[insert lines if needed]		

HAZARDS GENERATED BY THE EXPERIMENT (if using fixed installation:) Hazards named in the document relevant for the fixed [COLLAPS, CRIS, ISOLTRAP, MINIBALL + only CD, MINIBALL + T-REX, NICOLE, SSP-GLM chamber, SSP-GHM chamber, or WITCH] installation.

Additional hazards:

Hazards	[Part 1 of experiment/ equipment]	[Part 2 of experiment/ equipment]	[Part 3 of experiment/ equipment]
Thermodynamic and fluidic			
Pressure	[pressure][Bar], [volume][l]		
Vacuum			
Temperature	[temperature] [K]		
Heat transfer			
Thermal properties of materials			
Cryogenic fluid	[fluid], [pressure][Bar], [volume][l]		
Electrical and electromagnetic			
Electricity	[voltage] [V], [current][A]		
Static electricity			
Magnetic field	[magnetic field] [T]		
Batteries	☐		
Capacitors	☐		

Ionizing radiation			
Target material [material]			
Beam particle type (e, p, ions, etc)			
Beam intensity			
Beam energy			
Cooling liquids	[liquid]		
Gases	[gas]		
Calibration sources:	□		
• Open source	□		
• Sealed source	□ [ISO standard]		
• Isotope			
• Activity			
Use of activated material:			
• Description	□		
• Dose rate on contact and in 10 cm distance	[dose][mSV]		
• Isotope			
• Activity			
Non-ionizing radiation			
Laser			
UV light			
Microwaves (300MHz-30 GHz)			
Radiofrequency (1-300 MHz)			
Chemical			
Toxic	[chemical agent], [quantity]		
Harmful	[chem. agent], [quant.]		
CMR (carcinogens, mutagens and substances toxic to reproduction)	[chem. agent], [quant.]		
Corrosive	[chem. agent], [quant.]		
Irritant	[chem. agent], [quant.]		
Flammable	[chem. agent], [quant.]		
Oxidizing	[chem. agent], [quant.]		
Explosiveness	[chem. agent], [quant.]		
Asphyxiant	[chem. agent], [quant.]		
Dangerous for the environment	[chem. agent], [quant.]		
Mechanical			

Physical impact or mechanical energy (moving parts)	[location]		
Mechanical properties (Sharp, rough, slippery)	[location]		
Vibration	[location]		
Vehicles and Means of Transport	[location]		
Noise			
Frequency	[frequency],[Hz]		
Intensity			
Physical			
Confined spaces	[location]		
High workplaces	[location]		
Access to high workplaces	[location]		
Obstructions in passageways	[location]		
Manual handling	[location]		
Poor ergonomics	[location]		

Hazard identification:

Average electrical power requirements (excluding fixed ISOLDE-installation mentioned above): [make a rough estimate of the total power consumption of the additional equipment used in the experiment]